



Evaluation of chitosan-Ag/TiO₂ nanocomposite for the enhancement of shelf life of chili and banana fruits

Sourav Kumar Singha^{a,c,*}, Sheikh Manjura Hoque^b, Harinarayan Das^b,
Md Abdul Alim^c

^a Bangladesh Food Safety Authority, Dhaka, 1000, Bangladesh

^b Materials Science Division, Atomic Energy Centre, Ramna, Dhaka, Bangladesh

^c Department of Food Technology and Rural Industries, Bangladesh Agricultural University, Mymensingh, 2202, Bangladesh

ARTICLE INFO

Keywords:

Chitosan-cellulose
Ag/TiO₂
Antimicrobial activity
Chili and banana storage
Active food packaging
Shelf life

ABSTRACT

Post-harvest losses of fruits and vegetables account for a large share of food waste in the world due to improper handling and packaging. By using the sol-gel method, Ag/TiO₂ nanocomposite was prepared in this study from micro-sized commercial TiO₂ powder and incorporated in a chitosan-cellulose matrix for the purpose of promising food packaging. The particle size and distribution of Ag nanoparticles (9.2437 nm size) confirmed their successful inclusion in the TiO₂ surface. The morphology of the package assured the successful and uniform disbursement of Ag/TiO₂ nanocomposite into the chitosan-cellulose matrix, which led to enhanced water resistance and photocatalytic activity. The developed package is proficient in hindering the growth of fecal coliform bacteria (*Esche (Escherichia coli)*) by 9 mm in the agar plate. Moreover, the efficient application of chitosan-Ag/TiO₂ nanocomposite in food coating and packaging was examined in extending shelf life, minimizing water loss, and preventing microbial infection during the storage of chili (up to 7 days at 37 °C) and banana, respectively. It can be concluded from the results that chitosan-Ag/TiO₂ nanocomposite-based food coating and packaging have competent potential for enhancing the shelf life of moist foods.

1. Introduction

The world is facing challenges in food production, safety, and emerging health risks due to long-term changes in temperature, humidity, rainfall patterns, and environmental pollution. On the other hand, inadequate food safety practices in farming, processing, transport, and unplanned industrialization caused environmental pollution. According to a few studies, 12.5 million tons of plastic were used to produce food globally, and food packaging is the third-biggest industry as well as the source of microplastic contamination in the food chain[1–4]. So now, the food packaging and distribution industries are seeking cost-effective cellulose-based alternative active packaging with biodegradable, good appearance, enough mechanical strength, barrier qualities, non-toxic, and sustainable packaging[5,6].

Active packaging comes in four varieties, according to their functions: migratory, non-migratory, release (emitting antibacterial and antioxidant substances), and scavenger (absorbing O₂, CO₂, moisture, etc.) [7]. As a white food coloring additive, TiO₂ is one of the most widely utilized reinforced nanoparticles (NPs) to develop active packages because it is abundant in all three crystallographic

* Corresponding author. Bangladesh Food Safety Authority, Dhaka, 1000, Bangladesh.

E-mail address: souravsingha1917@gmail.com (S.K. Singha).

<https://doi.org/10.1016/j.heliyon.2023.e21752>

Received 14 October 2023; Accepted 26 October 2023

Available online 28 October 2023

2405-8440/© 2023 The Authors. Published by Elsevier Ltd. This is an open access article under the CC BY-NC-ND license (<http://creativecommons.org/licenses/by-nc-nd/4.0/>).

forms (anatase, rutile, and brookite). The most investigated photocatalytic materials, TiO₂ NPs with 80 % anatase and 20 % rutile have high photocatalytic activity[8]. On the other hand, TiO₂ only exhibits photocatalytic activity when exposed to UV light by creating reactive oxygen species (OH, H₂O₂, O₂)[9,10]. By doping TiO₂ or forming nanoparticles, it can be activated under visible light[11]. Different studies showed increasing photocatalytic and antimicrobial activity under visible light by doping TiO₂ with Fe, Au/Au³⁺, Pt, Ag, Cu, W, etc. [12–14]; F. B. [15]; X. Z [16]. Incorporation of chitosan and Ag with TiO₂ exhibits antimicrobial activity against the Gram-negative bacteria *Escherichia coli* and the Gram-positive bacteria *Staphylococcus aureus*, as well as different species of food-deteriorative yeast and fungus as well (*Candida albicans* and *Aspergillus niger*)[17–19].

[20] reported that there are six food packaging companies in the world now that produce active packages incorporating Ag-NPs in food containers to prolong the shelf life of food. Also, nano clay, nano-zinc oxide (nano-ZnO), nano-titanium dioxide (nano-TiO₂), and titanium nitride-NPs (nano-TiN) are used to produce food packages in the market[21]. Due to its wide range of shelf-life-enhancing properties, nano food packaging is getting attention on the market. In some studies, Ag/TiO₂ nanocomposite films were developed as antimicrobial agents [22,23] and cellulose-based films were developed by reinforcing Ag/TiO₂ nanocomposite to increase the shelf life of butter and walnut kernels [24,25]. In the previous studies, Ag/TiO₂ nanocomposite-based packages were developed using nanoTiO₂ as a precursor. Moreover, there are no studies for the preservation of food of high water activity (e.g. raw vegetables, fruits, or meats) with Ag/TiO₂-coated cellulose paper. As a food contact material, it is challenging for cellulose-based biodegradable packages to hinder moisture transfer between moist layered foods as well.

Therefore, the purpose of the current work is to develop chitosan-Ag/TiO₂ nanocomposite using microsized, commercial grade TiO₂ powder as a precursor and evaluate its application as food coating and active packaging. First of all, chitosan (Ch), chitosan-TiO₂ (Ch-TiO₂), and chitosan-Ag/TiO₂ (Ch-TiO₂) coating solutions were prepared. The uncoated paper (P) and three packages developed by coating cellulose-based paper sheets with the prepared solution: chitosan (P-Ch), chitosan-TiO₂ (P-Ch-TiO₂), and chitosan-Ag/TiO₂ (P-Ch-Ag/TiO₂), were characterized and assessed. Both photocatalytic activity and Fourier-transform infrared spectroscopy (FTIR) analysis of fresh (P-00, P-Ch-00, P-Ch-TiO₂-00, and P-Ch-Ag/TiO₂-00) and 04 month-aged (P-04, P-Ch-04, P-Ch-TiO₂-04, and P-Ch-Ag/TiO₂-04) packages were analyzed as well. By considering the context of Bangladesh the two moist foods, chili and banana were selected for evaluation of shelf life, which are consumed directly in hotels or restaurants without any further preparation and have high post-harvest loss rates. On the other hand, considering the unhygienic handling of these foods, a fecal coliform group bacteria *Escherichia coli* was used in this study to check the microbial susceptibility.

2. Materials and methods

2.1. Materials

The cellulose paper was bought from Bashundhara Paper Mills Limited, Bangladesh. Chitosan with a degree of deacetylation of 70 % was purchased from Research Lab Fine Chemical Industries (Mumbai, India). Commercial (Inframat Advanced Materials) rutile TiO₂ (.2 μm size) powder, AgNO₃, glycerol, Methyl Orange (Merck-Germany), and acetic acid (Merck-Germany) were used as raw materials for coating solutions. The bacterial strain *Escherichia coli* ATCC8099 was used to check the antibacterial activity of the developed packages.

2.2. Development of Ag-doped TiO₂ (Ag/TiO₂) nanocomposite

2.2.1. Formulation

Ag-doped TiO₂ nanocomposite was prepared according to the sol-gel method where TiO₂ powder and AgNO₃ were precursors. It was prepared by stirring 30 g of TiO₂ powder with a 0.05 M, 150 mL solution of AgNO₃ at 400 rpm for 24h. After filtration, this mixture was then evaporated to dryness at 120 °C until a constant weight was reached. Then the obtained precursor was calcined at 600 °C for 24h in the Muffle Furnace. To wash out the ions and other by-products formed during the reaction, the calcined powder was then washed at least four times with distilled water. After washing, the powder was dried at 120 °C in an oven for 24 h. To get a small size of Ag-doped TiO₂ nanocomposite, a mortar and pestle was used for grinding the obtained powder for 6 h

2.2.2. Characterization of structural properties

The phase analysis was done using a Phillips (PW3040) X-Pert PRO X-ray diffractometer. From the X-ray diffraction pattern, the crystallite grain size was determined by utilizing Scherer's equation as follows[26]:

$$D = \frac{K\lambda}{\beta \cos \theta}$$

where, D = Grain size.

K = a dimensionless shape factor with a value of unity. The factor has an atypical value of about 0.94

λ = value of λ is 1.54060Å^o for Cu-Kα radiation

β = Full Width Half Maxima (FWMH) of the peak for higher absorption than the rest from the X-ray diffraction pattern.

To determine the particle size and particle distribution of Ag/TiO₂, the Transmission Electron Microscopy (TEM) model of HT7800 Ruli TEM operated at 120 kV was used.

2.3. Preparation of cellulose-based active package

2.3.1. Preparation of coating formulation

The three coating solutions were developed for three coated packages following previous studies[25,27]. 75g of commercial chitosan powder was dissolved slowly in 50 mL of a 2 % (v/v) acetic acid solution under continuous stirring for 3 h. Thus, three sets of separate solutions were prepared. For the preparation of the (1) chitosan coating solution: only 2 mL of glycerol (as plasticizer); (2) chitosan-TiO₂ coating solution: 3.15 g of commercial TiO₂ power and 2 mL of glycerol; and (3) chitosan-Ag/TiO₂ coating solution: 3.15 g of prepared Ag/TiO₂ nanocomposite and 2 mL of glycerol were added to the three sets of solutions under continuous stirring until the mixture of all components.

2.3.2. Development of coated active package

Food-grade cellulose paper sheets (Basundhara Group) were used for coating by using the dip coating technique. The papers were cleaned with 80 % acetone solution and dried at room temperature (26 °C). The papers were cut into pieces with a diameter of 9.5 cm and dipped into the prepared different sol-gel solution for 1 min. The P-Ch, P-Ch-TiO₂, and P-Ch-Ag/TiO₂ packages were dried at room temperature for 24h and conditioned at 52 % relative humidity for 72h at 25 °C in a desiccator. Uncoated cellulose paper (P) treated with 2 % acetic acid was used as a control for further comparison.

2.4. Evaluation of active package

2.4.1. Surface morphology

An electron microscope (SEM) (Ven Ground) of 1200 mm (x400, x600) operated at an accelerating voltage of 30 kV was used for the morphological characterization of fresh and aged packages. An Energy Dispersive X-ray (EDX) detector attached to the scanning electron microscope conducted the elemental composition analysis of the investigated packages.

2.4.2. Fourier transform infrared spectroscopy (FTIR)

Fourier-transform infrared spectroscopy (FTIR) (Model: STE 449 F3 Jupitar) is a technique used to obtain the structural changes that occurred in the packages during their 4-month aging.

2.4.3. Photocatalytic activity

The photocatalytic efficiency of active packages was determined by exposing under ultraviolet light (UV) lamp that radiates light at a wavelength of 254 nm (UV-C band). Prepared coated and uncoated paper packages were cut into pieces of 4 cm by 4 cm and immersed in 500 mL of Methyl Orange (MO) solution with a concentration of 20 ppm. For adsorption, the solutions with the packages were maintained in the dark for 1h. The immersed packages were then exposed under a UV lamp for 20 min, and the degradation of MO in the solution was measured four times. The degradation of MO was calculated at 484 nm (Lambda 35 spectrophotometer, Perkin-Elmer). A linear regression equation ($R^2 = 0.9859$) was developed from the calibration curve of the absorbance of MO as follows[8]:

$$C_{MO} = \frac{Abs_{484}}{.0293}$$

where, C_{MO} is the concentration of the MO in the solution, in ppm; Abs_{484} is the absorbance of the solution at 484 nm; 0.0293 is the slope of the calibration curve. Then, by identifying the changes in initial and concentration after 20 min (C_i/C_o), the photodegradation of MO dye was calculated.

2.4.4. Water vapor transmission rate (WVTR)

80 × 80 mm of each package was fixed on top of the opening of a plexiglass test tube containing 10 g of silica gel. Each sample was properly sealed with vacuum grease on top of the test tube. Then test tubes with coated and uncoated packages samples were placed into a desiccator with distilled water (100 % humidity), and the whole set of test tubes was kept at (25 ± 0.5) °C, 50 % RH. The tubes were weighed for 4 days, and the weight gained was plotted versus time (the associated regression coefficients were in the range of 0.91–0.95)[28]. WVTR of the prepared packages was determined as:

$$WVTR \text{ (g/h. m}^2\text{)} = \frac{m}{\Delta t A}$$

where, WVTR is the water vapor transmission rate (g/h. m²); $\frac{m}{\Delta t}$ is the amount of water gain per unit time g/h; and A is the permeation area (2.2698 cm²).

2.4.5. Water absorption ability (WA) and water solubility (WS)

For testing of water absorption ability and water solubility, square-shaped specimens were cut using a scissor with a surface area of 400 mm² and dried for 24 h in an electric oven at 100 °C until the weight remained constant to consider the initial dry weight (W_1) to the nearest of 0.0001 g. Then, the precisely weighed dried packages were placed in a beaker (250 mL) containing 30 mL of 30 °C distilled water for 24 h. Package specimens were then removed to gently wipe out excess water from the surface of the packages with filter paper to measure the wet weight (W_2). Water solubility was calculated from the percentage weight gain of the wet weight to the

final dry weight (W_3)[29]. Percentages of water absorption ability and water solubility were calculated by:

$$\text{Water Absorption Ability (\%)} = \frac{W_2 - W_1}{W_1} \times 100$$

$$\text{Water solubility (\%)} = \frac{W_1 - W_3}{W_1} \times 100$$

2.4.6. Antibacterial activity

The antimicrobial efficiency of coated and uncoated packages was determined by the Kirby-Bauer disk diffusion method[30]. The three coated packages were cut into disks of 6 mm diameter before the experiment and an uncoated disk of the same size was considered as the control sample. Subsequently, the samples were sterilized using a UV light for 3 min under a biosafety cabinet. The *Escherichia coli* was then inoculated on the Eosin Methylene Blue (EMB) and Muller-Hinton (MH) agar plates by streaking the swab and allowing it to dry. Further, each disk of packages was placed on the specific portion of inoculated agar, and the plate was incubated at 37 ± 1 °C for 24 h. Ceftriaxone (30 mcg) antibiotic was used, and the bacteria-free zone (inhibition zone) was measured to the nearest mm.

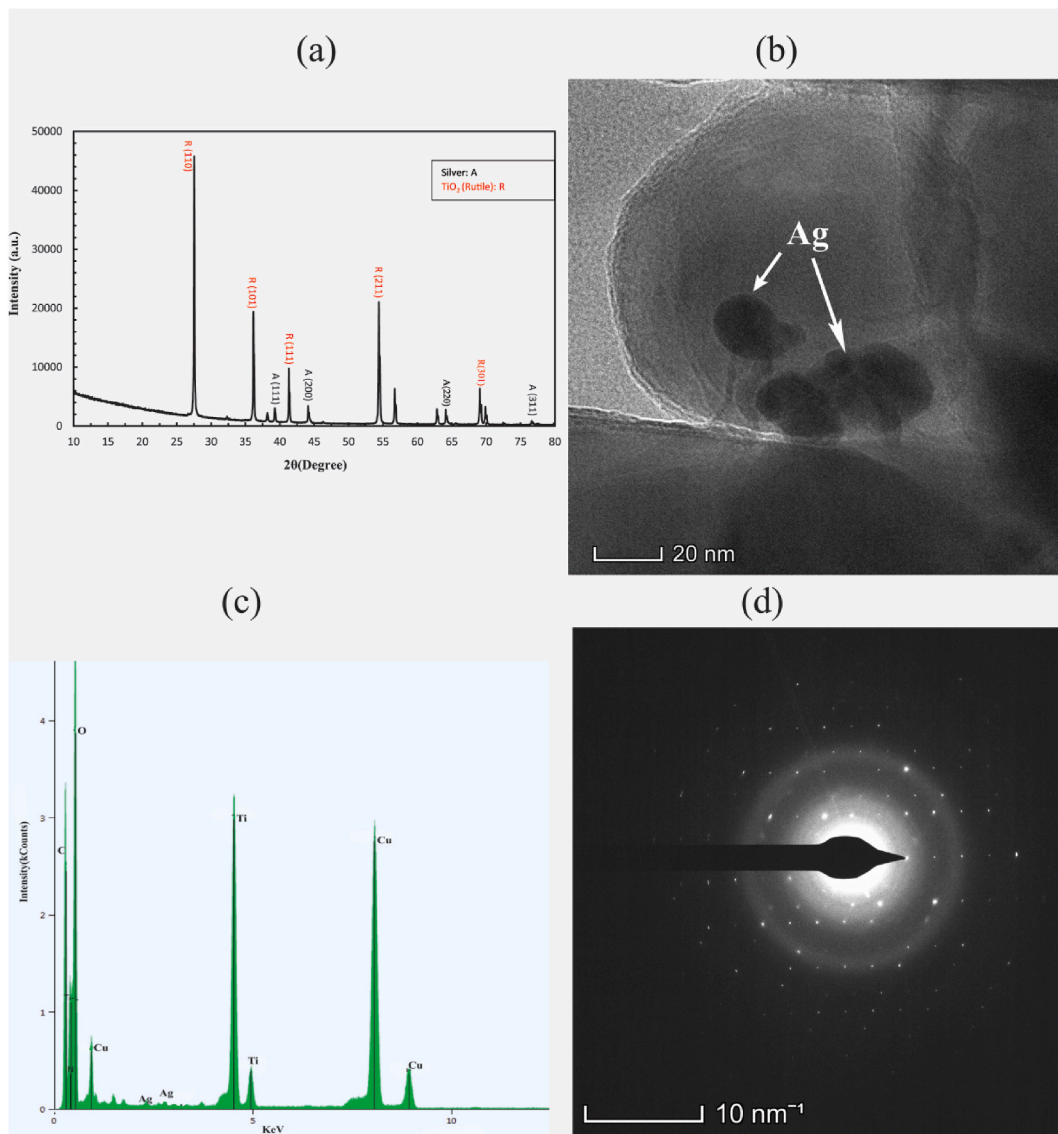


Fig. 1. (a) XRD patterns of the synthesized Ag/TiO₂ nanocomposite where Ag nanoparticle peak located at (111), (200), (220), (311) plane and TiO₂ peak located at (110), (101), (111), (211), (301) plane (b) TEM image of Ag decorated TiO₂ nanostructures (c) EDX pattern of Ag/TiO₂ nanocomposite (d) SAED of Ag/TiO₂ nanocrystals.

2.5. Shelf life evaluation

2.5.1. Effects of coating solution for the storage of chili

To validate the performance of the developed solutions of Ch, Ch-TiO₂, and Ch-Ag/TiO₂ the coating was performed by dipping fresh chili (*Capsicum frutescens* L) in the solutions for around 30 s at room temperature. Fresh chilies were collected from local farmers during harvesting and it was ensured that no chemicals were used or treated for long-term preservation and no adhered dirt on their skins [31]. After sterilization with 80 % ethanol and dipping, the coated chilies were dried and stored at 25/19 °C (light/night) and 50 % relative humidity until a consistent weight was gained for the uncoated chili. The percentage of weight loss was calculated in comparison with the initial weight of chilies. The mean values of replications were reported for control and treatment samples.

2.5.2. Effectivity of coated active package for packaging fresh banana

The prepared four-coated and uncoated packages of 10 cm in diameter were used to check the effectiveness of active packages. Fresh bananas (*Musa cavendishi*) were procured from the local market. A fresh, untreated banana was cut into 4 pieces precisely around the size of 3 cm in diameter. All the slices were put into coated and uncoated packages. The uncoated package (P) was considered a control. The packed banana slices were then stored at 4–7 °C in a refrigerator for 10 days. Weight loss during storage of each package was calculated as a percentage of weight loss.

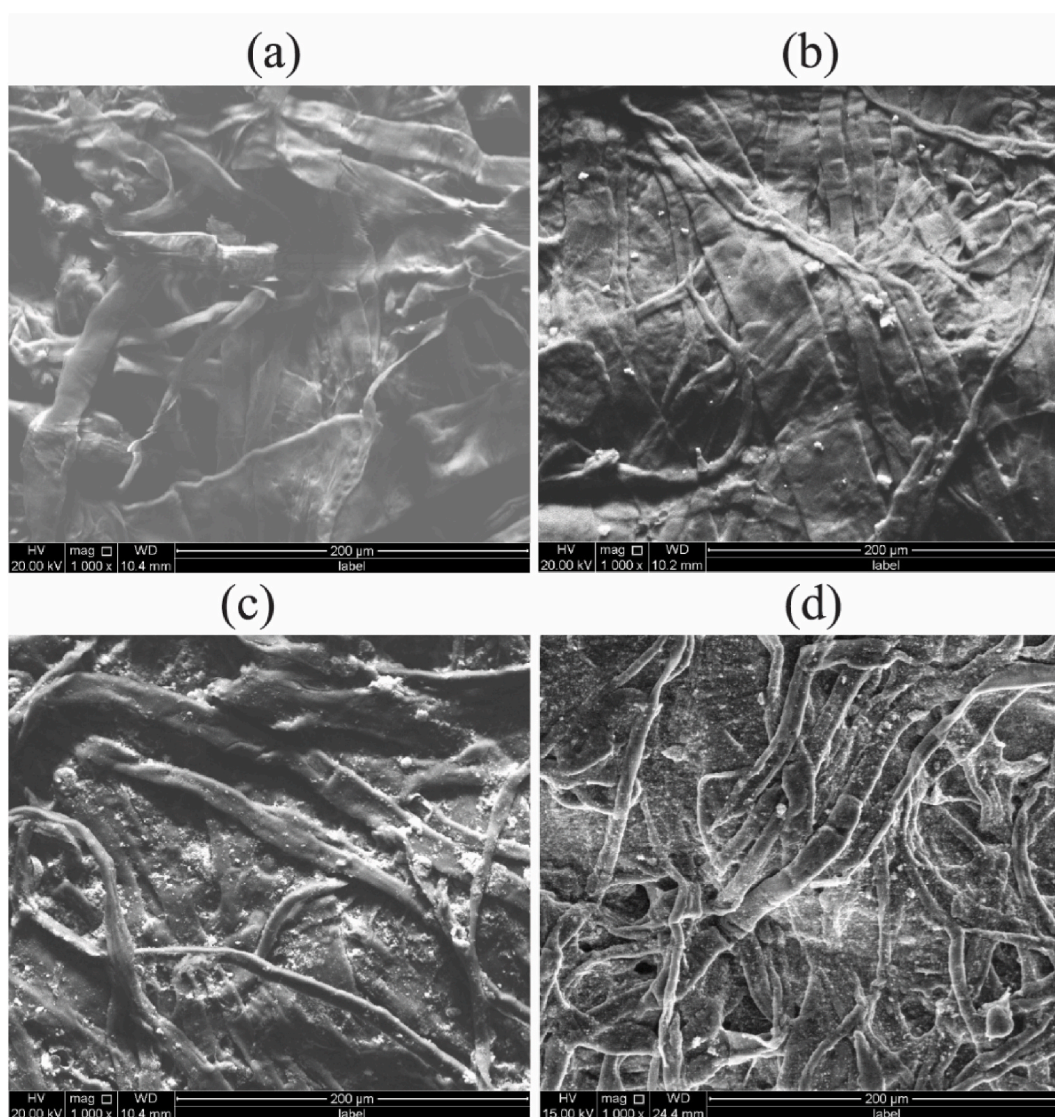


Fig. 2. Scanning electron microscopy micrographs of (a) P (b) P-Ch (c) P-Ch-TiO₂ (d) P-Ch-Ag/TiO₂ at 1000× magnification.

2.5.3. Microbiological analysis of stored chili and banana

By removing a tiny sample (5 g) from the fresh and stored chili and banana, the total number of bacteria and the total number of yeast and fungi were assessed. The samples were homogenized after being aseptically transferred into a sterile 0.1 % (w/v) peptone-NaCl solution. After the serial decimal dilutions in the solution, an aliquot of 5 μ L was spread in distinct petriplates containing nutrient and potato dextrose agar[32]. Following this, the inoculated petriplates underwent a separate 48-h incubation at 37 $^{\circ}$ C. The total bacterial count and total yeast and fungal counts, before and after storage, were used to calculate the percentage inhibition of growth on chili and bananas[24].

2.6. Experimental design and statistical analysis

For the experiment, the data obtained on the characteristics of different coated and uncoated packages and the shelf life of chili and bananas were statistically analyzed using IBM SPSS Statistics software, version 26. The means for all the treatments were calculated, and the analysis of variances (ANOVA) for all the parameters was performed by the F-test. The significance of the difference between the pair of means was compared using the Tukey test ($p \leq 0.05$).

3. Results and discussion

3.1. Structural properties of Ag/TiO₂ nanocomposite

Fig. 1a shows the XRD patterns of the Ag/TiO₂ nanocomposite. Diffraction peaks located at $2\theta = 27.54, 36.18, 41.32, 54.04,$ and 69.1 are assigned to the (110), (101), (111), (211), and (301) lattice planes of TiO₂, which indicate rutile phase (JCPDS Card No. 21-1276)[33]. The Ag nanoparticle peaks located at $2\theta = 38.16, 44.16, 64.24,$ and 77.54 are assigned to the FCC structure ascribed to the (111), (200), (220), and (311) planes. That exhibits a fine crystal structure of Ag/TiO₂. The highest peak in the XRD patterns, the miller indices (110) is the value for FWHM. Using Scherer's equation, the calculated crystallite grain size for the respective peak is 17.88 nm.

Fig. 1b shows the TEM images of the synthesized Ag/TiO₂ nanocomposite. Ag nanoparticles aggregated into Ag clusters and were distributed on the surface of the TiO₂ particles, as was observed. Furthermore, dispersive Ag nanoparticles around the Ag cluster identified no agglomeration[34]. Also, in Fig. 1b, the calculated size of silver nanoparticles was 9.2437 nm each. Fig. 1c shows the EDX elemental mapping of the Ag/TiO₂ with a clear demarcation of the presence of silver nanoparticles on the surface of TiO₂. However, the ratio of Ag nanoparticles in comparison with Ti and O was less. In Fig. 1d, the Selected Area Electron Diffraction (SAED) displayed concentric diffraction rings that suggest the composites' polycrystalline structure[35]. XRD and TEM images show the uniform distribution and strong interaction between Ag and TiO₂ which will active micro-sized TiO₂ to act as strong antimicrobial agents.

3.2. Morphology of coated active package

Fig. 2 shows the SEM of the surface and cross sections of P, P-Ch, P-Ch-TiO₂, and P-Ch-Ag/TiO₂ active packages. The distribution of chitosan, micro-sized TiO₂, and Ag/TiO₂ NPs microstructure and elemental composition of the active packages were also evaluated. As depicted in Fig. 2a, on the surface of P, there was a clear demarcation of fibers at a 200 μ m scale. The surface of the fresh package was uniform in shape, with a size of several microns. There was nothing unusual or damaged about the fiber but some pores. After coating, the porosity of cellulose packages decreased and the fibers tied together properly, resulting in better barrier properties. In addition, the chitosan molecules (Fig. 2b) were on the surface of the package and observed a clear distinction between the P and P-Ch. Chitosan existed as aggregates both in pores and on the surface of packages. The distribution of chitosan molecules on the surface was not uniform which might be due to the dip-coating procedure used to prepare the packages. As compared to P-Ch (Fig. 2c and d), ample amounts of TiO₂ and Ag NPs were seen scattered on the surfaces of P-Ch-TiO₂ and P-Ch-Ag/TiO₂ packages. TiO₂ and Ag/TiO₂ nanocomposites were properly bound with cellulose fiber and incorporated into the chitosan matrix.

The EDX technique was used to present the elemental mapping of P, P-Ch, P-Ch-TiO₂, and P-Ch-Ag/TiO₂ in Table 1. In every coated and uncoated package, carbon and oxygen were the main elements and the weight percentages of the two elements in P were 55.22 % (62.21 at%) and 44.73 % (37.79 at%), respectively [36]. The presence of N (4.80 wt%) was due to chitosan associated with the NH₂ group in P-Ch. That was the clear demarcation between the incorporation of chitosan and bonding with the cellulose fiber properly [36]. Also, the existence of N was found in the P-Ch-TiO₂ and P-Ch-Ag/TiO₂ samples, which proved the existence of chitosan in the active packages. The existence of Ti and Ag was due to the addition of TiO₂ powder and Ag/TiO₂ nanocomposite to the cellulose

Table 1
Elemental Composition of prepared packages obtained by Energy Dispersive X-ray (EDX) method.

	C		O		N		Ti		Ag	
	at. %	wt %	at. %	wt %	at. %	wt %	at. %	wt %	at. %	wt %
P	62.21	55.22	37.79	44.73						
P-Ch	55.42	48.32	39.30	45.70	4.71	4.80				
P-Ch-TiO ₂	43.29	27.14	39.10	32.70	1.61	1.18	14.70	36.80		
P-Ch-Ag/TiO ₂	27.97	17.23	54.18	44.43	3.20	2.29	13.95	34.25	0.19	1.02

matrix. In Table 1, the weight percentage of elements in P-Ch-TiO₂ (C = 27.14 %, O = 32.70 %, N = 1.18 %, Ti = 36.80 %) and P-Ch-Ag/TiO₂ samples (C = 17.23 %, O = 44.43 %, N = 2.29 %, Ti = 34.25 %, Ag = 1.02 %) showed that the amount of TiO₂ was around 35 % in overall composition. On the contrary, due to the attachment of nano-sized Ag in the TiO₂ matrix, the P-Ch-Ag/TiO₂ package might show high photocatalytic activity and exhibit antimicrobial properties.

3.3. Fourier transform infrared spectroscopy (FTIR)

Fig. 3 shows a comparative investigation using FTIR of fresh and 4-month-aged coated and uncoated active packages. In the 1500 and 800 cm⁻¹ regions (Fig. 3a), uncoated fresh (P-00) and 4-month-aged packages (P-04) are similar in absorbance. However, there are changes observed at the broad band in 3500–3000 cm⁻¹ which correspond to the O–H stretching [27]. The higher stretching of P-04 at the 3332 cm⁻¹ band than P-00 indicates that the package absorbed moisture from the environment and established new hydrogen bonds between the cellulose chains during aging. As shown in Fig. 3b, there are broader absorbance bands in chitosan-coated fresh (P-Ch-00) and aged (P-Ch-04) packages at the 3500–3000 cm⁻¹ due to the presence of amino (N–H) and hydroxyl (O–H) groups. The two overlapping groups distinguish chitosan-based packages from P and chitosan. Similarly, the stretching bands (3500–3000 cm⁻¹) in P-Ch-TiO₂-00, P-Ch-TiO₂-04, P-Ch-Ag/TiO₂-00, and P-Ch-Ag/TiO₂-04 prove the presence of chitosan in those packages (Fig. 3c). Due to the internal change of chitosan (N-deacetylation) during aging, P-Ch-Ag/TiO₂-04 shows lower absorbance in the above-mentioned

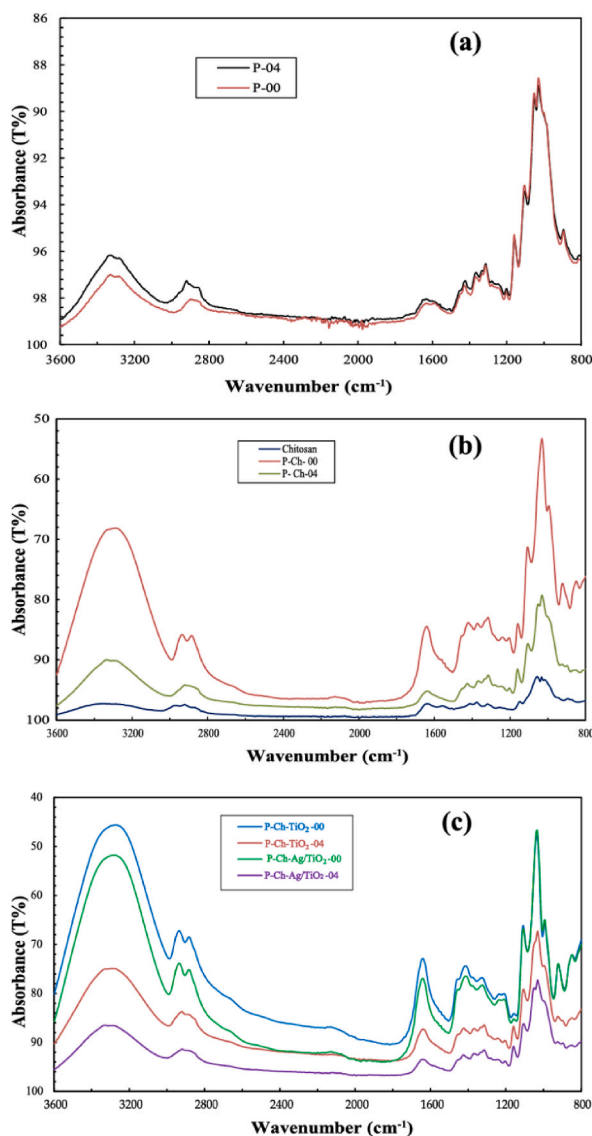


Fig. 3. FTIR spectra of (a) fresh P-00 and 4-month aged P-04, (b) fresh P-Ch-00 and 4-month aged P-Ch-04, (c) fresh P-Ch-TiO₂-00, P-Ch-Ag/TiO₂-00 and 4-month aged P-Ch-TiO₂-04, P-Ch-Ag/TiO₂-04 package.

region[24].

The band in the region of 3000–2800 cm^{-1} represents the functional group of C–H stretching vibrations in the aliphatic hydrocarbons of cellulose[37]. The two significant peaks at 2922 and 2896 cm^{-1} are noticed as $-\text{CH}_2$ and $-\text{CH}_3$ stretching. The two identified peaks may indicate the binding of chitosan and cellulose to each other (Fig. 3a). Due to the contribution of molecular groups of cellulose and chitosan, the spectrum around the region of aliphatic hydrocarbons has become broader in P-Ch-04 (Fig. 3b). The peaks at around 1155 cm^{-1} and 1032 cm^{-1} correspond to the polysaccharide structure of chitosan[27]. The C=O (carbonyl) stretching and the stretching vibrations of the amino group (amide bands) of the amino acetyl group of chitosan are attributed to the absorbance peaks between 1650 and 1560 cm^{-1} , which demonstrate that the initial chitosan was not entirely deacetylated[25]. Similarly, as seen in Fig. 3c, the FTIR spectra for fresh and 4-month-aged P-Ch-TiO₂ and P-Ch-Ag/TiO₂ packages display shifting peaks at 1642 cm^{-1} (C–O stretching) to a higher value than the chitosan-coated package, which proves the inclusion of TiO₂ and Ag/TiO₂ in the chitosan-cellulose matrix. By comparing aged P-Ch-TiO₂ and P-Ch-Ag/TiO₂ packages in the band stretching 1700 to 1594 cm^{-1} wave numbers, a broader weak peak is observed for P-Ch-Ag/TiO₂-04 packages that indicate the disruption of the cellulose-chitosan matrix. Because the nano-Ag NPs exhibited high photocatalytic activity due to exposure to visible light during storage.

3.4. Photocatalytic activity

TiO₂ and Ag/TiO₂ are photocatalysts that show photocatalytic activity during exposure to UV light and generate electrons and holes. An active surface reaction between the Methyl Orange (MO) dye and TiO₂ catalyst accelerates the photocatalytic degradation [38]. The degradation rates of Methyl Orange as a marker of the photocatalytic activity of the packages investigated are displayed in Fig. 4.

Initially, the adsorption of dye in fresh P-Ch, P-Ch-TiO₂, and P-Ch-Ag/TiO₂ and aged P-Ch-04, P-Ch-TiO₂-04, and P-Ch-Ag/TiO₂-04 was measured in the dark. The results showed that the highest degradation of dye caused by aged and fresh P-Ch-Ag/TiO₂ among the packages was 5.71 % and 4.3 %, respectively[39]. While for P-Ch-TiO₂, the degradation of dye was 45.18 % less than fresh P-Ch-Ag/TiO₂. The adsorption percentage of MO dye for P-Ch was negligible.

By calculating C_t/C_0 for all the packages, the photodegradation of MO remained at the plateau stage until the end of the experiment after exposure to UV for 60 min[40].

As shown in Fig. 4, after 60 min, P-Ch exhibited lower photocatalytic activity than others, with 23.03 % absorption of MO dye. On the other hand, by incorporating TiO₂ and Ag/TiO₂ with chitosan-coated packages, the photocatalytic activity increased notably by 23.64 % and 34.34 %, respectively. Several studies confirmed that the incorporation of Ag/TiO₂ nanocomposite increased photocatalytic activity[41]. The doping of silver ions in the TiO₂ matrix increases the surface area and small particle size, which have a large contribution to the synergistic effect of capturing more incident light and transmitting photogenerated electrons[42]. MO decomposition rates for 4-month-aged packages were higher than those for fresh packages: 42.13 % for P-Ch, 48.06 % for P-Ch-TiO₂, and 63.06 % for P-Ch-Ag/TiO₂. The reason for the higher photocatalytic activity may be due to chitosan and cellulose, which may cover the active sites of TiO₂ and Ag/TiO₂ in fresh packages[24,42]. Due to the N-deacetylation of chitosan, the active sites may open during four months of storage. In our study, it can be concluded from FTIR spectra that the chitosan-cellulose matrix was disrupted, which boosted the photocatalytic activity of aged packages.

3.5. Water resistibility

Table 2 shows the swelling and water solubility of P-Ch, P-Ch-TiO₂, and P-Ch-Ag/TiO₂ active packages in distilled water (30 °C).

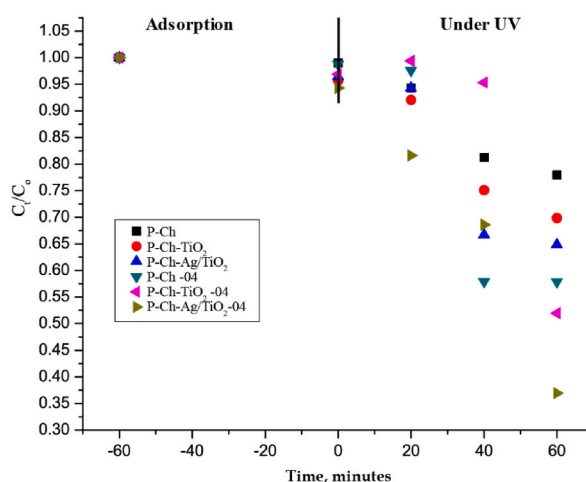


Fig. 4. Decomposition of Methyl Orange dye in the prepared fresh coated (P-Ch, P-Ch-TiO₂, P-Ch-Ag/TiO₂) and 4-month aged coated (P-Ch-04, P-Ch-TiO₂-04, P-Ch-Ag/TiO₂-04) packages during exposure to dark and UV irradiation.

Cellulose is not soluble in water, so P ($6.65 \pm 1.041\%$) expressed the minimum solubility, which also exhibited the highest absorption ability ($68.95 \pm 1.78\%$). The solubility of packages increased after the incorporation of chitosan into the cellulose matrix. Because chitosan is a natural cationic polymer, it can degrade [43]. Due to the physiochemical reaction between chitosan and cellulose, partial elimination of the hydroxyl group might occur. That might be the cause of the reduced water absorption ability of P-Ch [29]. The significant water absorption caused by P-Ch-Ag/TiO₂ was $75.98 \pm 0.91\%$ due to degradation of the cellulose and chitosan layers. After incorporating Ag/TiO₂ nanocomposite into the cellulose-chitosan matrix, it disrupted the hydrogen bonds, which supports the FTIR result. A previous study supports the findings that the addition of Ag to the chitosan matrix increased water swelling [28]. On the other hand, P-Ch-Ag/TiO₂ ($10.52 \pm 1.59\%$) exhibited less solubility [44]. showed that the incorporation of Ag nanoparticles in starch films extends the electrostatic interactions between polymeric chains and the hydrophobic nature of the film, which reduces film solubility. Also, it can be proven that TiO₂ and Ag/TiO₂ perfectly bind with the chitosan matrix. The low water solubility of food packaging materials is important for sustainable packaging [45].

The coatings of chitosan, TiO₂, and Ag/TiO₂ have significant effects on the water vapor transmission rate, as shown in Table 2. Due to the reduction of pores after coating, the coated cellulosic packages acted as a strong water vapor barrier. The P-Ch-Ag/TiO₂ showed the highest water vapor barrier properties [46]. reported that the WVTR of low-density polyethylene (60 wt% silica gel) was $18.8 \pm 0.7\%$, which was slightly lower than the WVTR of the P-Ch-Ag/TiO₂ package ($24.23 \pm 3.48\%$) from our study. The P-Ch-Ag/TiO₂ package exhibited a 16.362 % lower WVTR than the cellulose package. The WVTR of the P-Ch-TiO₂ package was higher than the P-Ch-Ag/TiO₂, which supports the previous study where the WVTR of Ag-incorporated films in chitosan was higher than the TiO₂-chitosan film [28]. Thus, it was concluded that the P-Ch-Ag/TiO₂ package contains high water-resistance properties, which might be introduced when storing highly moist food.

3.6. Antibacterial properties of active packages

Fig. 5 shows the clear demarcation of antimicrobial activity of the developed active packaging materials, which also imitate the antimicrobial scenario during food storage. The antibacterial activity of P, P-Ch, P-Ch-TiO₂, and P-Ch-Ag/TiO₂ was investigated by the Kirby-Bauer disc diffusion method. The effectiveness of the package was tested against the most common pathogen, *Escherichia Coli*. The uncoated fresh packages P and P-Ch did not show any inhibition zones. A study reported that chitosan-coated cellulose packages did not exhibit any inhibition zone against *Listeria monocytogenes* [27]. On the other hand, the inhibition zone of the chitosan-TiO₂-coated package (P-Ch-TiO₂) against *Escherichia Coli* bacteria was zero as well. The bactericidal properties of TiO₂ depend on the photocatalytic reaction that happens under UV radiation and produces reactive radicals [47]. So during the incubation period, TiO₂ exhibited no antibacterial activity [18]. reported that no inhibition zone of TiO₂ thin film was determined under dark conditions. But the Ag/TiO₂-incorporated package showed the highest inhibition against *Escherichia Coli*. Similarly, the chitosan-Ag/TiO₂ coated package (P-Ch-Ag/TiO₂) exhibited significant antimicrobial activity in our study. In comparison with CTR Ceftriaxone antibiotics, the inhibition zone of P-Ch-Ag/TiO₂ was 12 mm and 9 mm in EMB and MH agar, respectively. It proved that P-Ch-Ag/TiO₂ is also sustainable under dark conditions, which may be useful during the transportation of light-sensitive or refrigerated food.

3.7. Shelf life of chili and banana

During storage of fresh chili and banana slices, coating solutions and coated packages showed effectiveness in enhancing shelf life, respectively (Figs. 6 and 7). Bacterial, Yeast and Mold growth inhibition and weight loss of chili and banana slices during storage are shown in Table 3. Fig. 6 a, b, c, and d illustrate the changes in physical appearance and weight loss of fresh chili during storage at 25-19 °C after removal of the coating. In Fig. 6 c, and d a few white silvery-like substances are seen on the surface of the chili which were the remainder of TiO₂ and Ag/TiO₂ powders. The uncoated chili was fully spoiled containing several moldy spots only after 4 days of storage. Ch-Ag/TiO₂-coated chili was a little bit ripe but still greenish and firm in structure. The weight loss of Ch-Ag/TiO₂-coated chili was $53.04 \pm 1.42\%$ during the 7 days of storage, where $62.56 \pm 0.86\%$ and $65.67 \pm 0.75\%$ of weight loss were calculated for Ch-TiO₂ and Ch-coated chili, respectively (Fig. 6e) [48]. demonstrated the reduced water loss of mango during 20 days storages by coating with chitosan-nano-TiO₂ [49]. also reported the successful inhibition of the growth of aerobic mesophilic bacteria on blueberries by coating chitosan-nano-TiO₂. Similarly, the growth inhibition of bacteria and growth inhibition of yeast and mold of Ch-Ag/TiO₂-coated chili was higher than the Ch-TiO₂. The inhibition of Ag/TiO₂-coated chili for bacteria was $91.59 \pm 3.08\%$ and yeast and mold inhibition was $87.76 \pm 3.12\%$ whereas without coating chili exhibited no inhibition (Table 3).

Fig. 7 shows similar findings during the storage of banana slices packed in four coated and uncoated packages for 10 days. Photos were taken on the 5th day of storage at 4–7 °C, as shown in Fig. 7 a, b, c, and d. The physical changes of packages were also observed

Table 2

Water absorption ability, solubility, and water vapor transmission rate of uncoated cellulose packages and coated packages.

Packages	WA (%)	WS (%)	WVTR (g/h. m ²)
P	68.95 ± 1.78^a	6.65 ± 1.41^a	24.23 ± 3.48^a
P-Ch	46.35 ± 1.89^b	34.53 ± 1.77^b	21.14 ± 2.76^{bc}
P-Ch-TiO ₂	26.47 ± 1.21^c	39.20 ± 1.83^b	22.90 ± 3.41^b
P-Ch-Ag/TiO ₂	$75.98 \pm .91^d$	10.52 ± 1.59^c	20.26 ± 2.83^c

*Means followed by the same superscript in a column were not significantly different ($P > 0.05$).

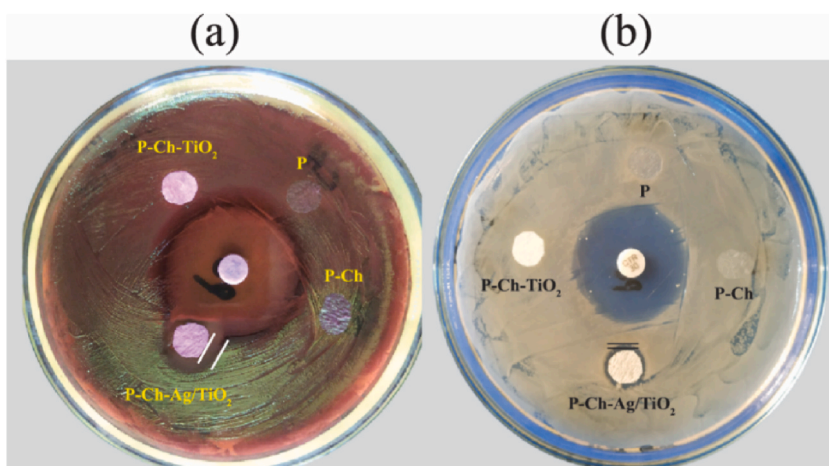


Fig. 5. Antibacterial activity of uncoated (P) and coated (P-Ch, P-Ch-TiO₂, P-Ch-Ag/TiO₂) packages against *Escherichia coli* in (a) EMB and (b) MH agar in comparison with CTR Ceftriaxone antibiotics in the middle of the plate.

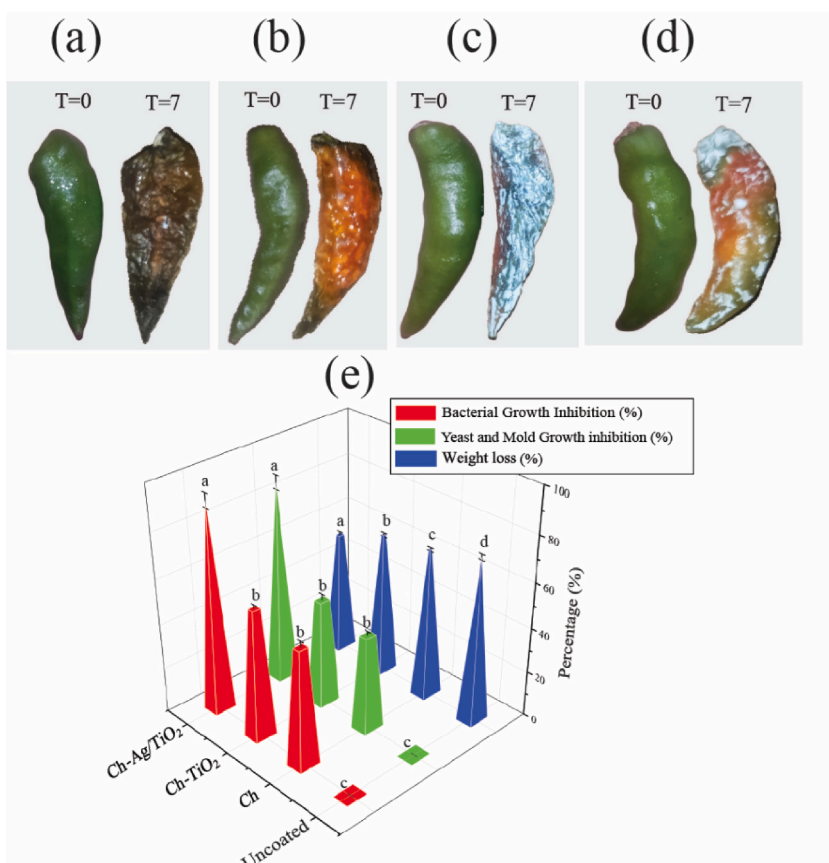


Fig. 6. Demonstration of physiological comparison of fresh (T = 0) and after 7 days stored (25-19 °C) chili (T = 7) (a) Uncoated and (b) Chitosan (Ch), (c) chitosan- TiO₂, (Ch - TiO₂) (d) chitosan- Ag/TiO₂ (Ch-Ag/TiO₂) coated solution; (e) Weight loss (%), inhibition of Bacteria, Yeast, and Mold (%) in comparison with uncoated and coating with prepared solutions.

*Means followed by the same letter were not significantly different (P > 0.05).

where the P and P-Ch surfaces were wet and the surfaces of the slices were visible from the outside. Because the two packages exhibited high WA and WVRT which might be the cause of quick soaking [29]. On the 5th day of storage, the appearance of P-Ch-Ag/TiO₂ was fresh and comparatively dry, which indicates the prevention of leakage of any substances from the surface of the banana slice.

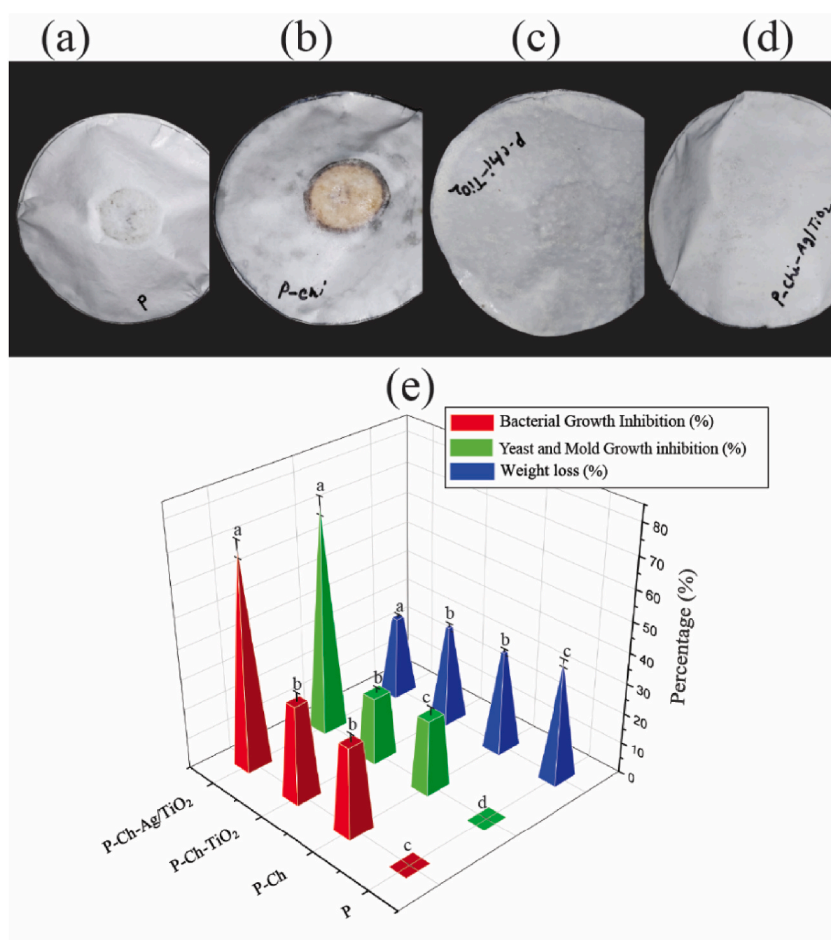


Fig. 7. Demonstration of physiological comparison of banana slice packaged with (a) P (b) P-Ch (c) P-Ch-TiO₂ (d) P-Ch-Ag/TiO₂ for 10 days storage (4–7 °C); (e) comparison of weight loss (%), inhibition of Bacteria, Yeast, and Mold (%) with different packages during storage.

*Means followed by the same letter were not significantly different ($P > 0.05$).

Table 3

Bacterial, Yeast and Mold growth inhibition and weight loss of chili and banana slices during storage.

Packages	Chili after 7 days of storing at 25–19 °C			Banana slices after 10 days of storing at 4–7 °C		
	Bacterial growth inhibition (%)	Yeast and Mold growth inhibition (%)	Weight loss (%)	Bacterial growth inhibition (%)	Yeast and Mold growth inhibition (%)	Weight loss (%)
P	0 ^a	0 ^a	72.39 ± 1.26 ^a	0 ^a	0 ^a	38.29 ± 1.30 ^a
P-Ch	51.77 ± 2.73 ^b	42.07 ± 1.73 ^b	65.67 ± .75 ^b	29.07 ± 2.68 ^b	24.13 ± 2.73 ^b	32.50 ± .99 ^b
P-Ch-TiO ₂	56.81 ± 1.75 ^b	46.58 ± 2.61 ^b	62.56 ± .86 ^c	31.58 ± 3.07 ^b	21.54 ± 1.81 ^c	31.72 ± 1.21 ^b
P-Ch-Ag/TiO ₂	91.59 ± 3.08 ^c	87.76 ± 3.12 ^c	53.04 ± 1.42 ^d	70.25 ± 2.85 ^c	73.42 ± 2.91 ^d	26.13 ± 1.15 ^c

*Means followed by the same superscript in a column were not significantly different ($P > 0.05$).

As shown in Fig. 7e, P-Ch-Ag/TiO₂ exhibited 34.27 % less weight loss during storage than P-Ch-TiO₂. The highest weight losses were also calculated for P due to the higher water vapor transmission rate. There was no significant difference in the weight loss and antimicrobial inhibition of P-Ch and P-Ch-TiO₂ packages. The bacterial growth inhibition and yeast and mold growth inhibition of banana in the P-Ch-Ag/TiO₂ package were higher than those in P-Ch-TiO₂ which were 55.04 % and 51.88 %, respectively (Table 3). The results indicate that large TiO₂ particles in the cellulose-chitosan matrix did not exhibit sufficient barrier and antimicrobial properties. Incorporation of Ag NP in TiO₂ released active compounds that attack bacterial cells leading to death and decomposition of the H₂O and O₂ entrapped in the package, which keeps the food safe [25,50]. The study validates that P-Ch-Ag/TiO₂ package is durable

for the long-term preservation of fresh vegetables by acting as a barrier to moisture transfer and microbial growth in high-moisture foods.

4. Conclusion

The study was designed to develop a cost-effective Ag/TiO₂ nanocomposite as a shelf life boosting material with water-resistant and antimicrobial properties. Also, the aim was to evaluate the effectivity of the nanocomposite as food coating and packaging materials by using commercial grade micro-sized TiO₂ powder as precursors. Cellulose-based active packages were simply dip-coated in chitosan (P-Ch), chitosan-TiO₂ (P-Ch-TiO₂), and chitosan-Ag/TiO₂ (P-Ch-Ag/TiO₂) solutions, respectively, and characterized in relation to uncoated package (P). After coating, compared with the uncoated package, the pores of the paper were filled finely, the surface of the package was smooth, and nothing unusual or damaged was noticed by using the SEM technique. The incorporation of a synthesized Ag/TiO₂ nanocomposite in a cellulose-chitosan matrix increased the water resistance and anti-microbial properties of packages. The developed P-Ch-Ag/TiO₂ package showed higher absorption ability, less solubility, and low water vapor, which are important properties for sustainable packaging materials. Among all packages, the Ag/TiO₂-coated active package exhibited the highest photocatalytic activity, which is the reason for the strong antimicrobial activity against the growth of *Escherichia Coli*. During the validation of coating solutions and coated packages, Chitosan-Ag/TiO₂ successfully showed minimum water loss, antimicrobial activity, and longer shelf life properties for moist foods during storage. The incorporation of Ag/TiO₂ nanocomposite in chitosan matrix with cellulose extends the effectiveness of the package and would be an excellent biodegradable food packaging material in the future.

Availability of data

All available data has been presented in the paper.

Funding

This research did not receive any specific grant from funding agencies in the public, commercial, or not-for-profit sectors.

CRedit authorship contribution statement

Sourav Kumar Singha: Conceptualization, Data curation, Formal analysis, Investigation, Methodology, Validation, Writing – original draft, Writing – review & editing. **Sheikh Manjura Hoque:** Formal analysis, Resources, Supervision, Writing – review & editing. **Harinarayan Das:** Resources, Software. **Md Abdul Alim:** Supervision.

Declaration of competing interest

The authors declare that they have no known competing financial interests or personal relationships that could have appeared to influence the work reported in this paper.

Acknowledgement

The authors acknowledge BAEC, Dhaka, and the Department of Microbiology, BAU greatly.

References

- [1] Assessment of Agricultural Plastics and Their Sustainability: A Call for Action, FAO, 2021, <https://doi.org/10.4060/cb7856en>.
- [2] N. Omerović, M. Džisalov, K. Živojević, M. Mladenović, J. Vunduk, I. Milenković, N.Ž. Knežević, I. Gadjanski, J. Vidić, Antimicrobial nanoparticles and biodegradable polymer composites for active food packaging applications, *Compr. Rev. Food Sci. Food Saf.* 20 (3) (2021) 2428–2454, <https://doi.org/10.1111/1541-4337.12727>.
- [3] B. Udovicki, M. Andjelkovic, T. Cirkovic-Velickovic, A. Rajkovic, Microplastics in food: scoping review on health effects, occurrence, and human exposure, *Int. J. Flow Control* 9 (1) (2022) 7, <https://doi.org/10.1186/s40550-022-00093-6>.
- [4] X. Zhao, K. Cornish, Y. Vodovotz, Narrowing the gap for bioplastic use in food packaging: an update, *Environ. Sci. Technol.* 54 (8) (2020) 4712–4732, <https://doi.org/10.1021/acs.est.9b03755>.
- [5] J.-W. Han, L. RuizGarcía, J.-P. Qian, X.-T. Yang, Food packaging: a comprehensive review and future trends: food packaging: review and future trends, *Compr. Rev. Food Sci. Food Saf.* 17 (4) (2018) 860–877, <https://doi.org/10.1111/1541-4337.12343>.
- [6] N. Noshirvani, B. Ghanbarzadeh, R. Rezaei Mokarram, M. Hashemi, Novel active packaging based on carboxymethyl cellulose-chitosan-ZnO NPs nanocomposite for increasing the shelf life of bread, *Food Packag. Shelf Life* 11 (2017) 106–114, <https://doi.org/10.1016/j.fpsl.2017.01.010>.
- [7] J.R. Westlake, M.W. Tran, Y. Jiang, X. Zhang, A.D. Burrows, M. Xie, Biodegradable active packaging with controlled release: principles, progress, and prospects, *ACS Food Science & Technology* 2 (8) (2022) 1166–1183, <https://doi.org/10.1021/acsfoodscitech.2c00070>.
- [8] Z. Qin, W. Liu, H. Chen, J. Chen, H. Wang, Z. Song, Preparing photocatalytic paper with improved catalytic activity by in situ loading poly-dopamine on cellulose fibre, *Bull. Mater. Sci.* 42 (2) (2019) 54, <https://doi.org/10.1007/s12034-019-1736-1>.
- [9] R.F. Hamilton, N. Wu, D. Porter, M. Buford, M. Wolfarth, A. Holian, Particle length-dependent titanium dioxide nanomaterials toxicity and bioactivity, *Part. Fibre Toxicol.* 6 (1) (2009) 35, <https://doi.org/10.1186/1743-8977-6-35>.
- [10] J. Xie, Y.-C. Hung, Methodology to evaluate the antimicrobial effectiveness of UV-activated TiO₂ nanoparticle-embedded cellulose acetate film, *Food Control* 106 (2019), 106690, <https://doi.org/10.1016/j.foodcont.2019.06.016>.
- [11] A. Jbeli, Z. Hamden, S. Bouattour, A.M. Ferraria, D.S. Conceição, L.F.V. Ferreira, M.M. Chehimi, A.M.B. Do Rego, M. Rei Vilar, S. Boufi, Chitosan-Ag-TiO₂ films: an effective photocatalyst under visible light, *Carbohydr. Polym.* 199 (2018) 31–40, <https://doi.org/10.1016/j.carbpol.2018.06.122>.

- [12] J.O. Carneiro, V. Teixeira, A. Portinha, L. Dupák, A. Magalhães, P. Coutinho, Study of the deposition parameters and Fe-dopant effect in the photocatalytic activity of TiO₂ films prepared by dc reactive magnetron sputtering, *Vacuum* 78 (1) (2005) 37–46, <https://doi.org/10.1016/j.vacuum.2004.12.012>.
- [13] A. Khlyustova, N. Sirotkin, T. Kusova, A. Kraev, V. Titov, A. Agafonov, Doped TiO₂: the effect of doping elements on photocatalytic activity, *Materials Advances* 1 (5) (2020) 1193–1201, <https://doi.org/10.1039/D0MA00171F>.
- [14] C. Lee, C. Kessler, M. Makris, J. Barback, *Haemophilia* 2010, *Haemophilia: The Official Journal of the World Federation of Hemophilia* 16 (1) (2010) 1–2, <https://doi.org/10.1111/j.1365-2516.2009.02168.x>.
- [15] F.B. Li, X.Z. Li, The enhancement of photodegradation efficiency using Pt–TiO₂ catalyst, *Chemosphere* 48 (10) (2002) 1103–1111, [https://doi.org/10.1016/S0045-6535\(02\)00201-1](https://doi.org/10.1016/S0045-6535(02)00201-1).
- [16] X.Z. Li, F.B. Li, Study of Au/Au³⁺-TiO₂ photocatalysts toward visible photooxidation for water and wastewater treatment, *Environ. Sci. Technol.* 35 (11) (2001) 2381–2387, <https://doi.org/10.1021/es001752w>.
- [17] Y. Xing, X. Li, X. Guo, W. Li, J. Chen, Q. Liu, Q. Xu, Q. Wang, H. Yang, Y. Shui, X. Bi, Effects of different TiO₂ nanoparticles concentrations on the physical and antibacterial activities of chitosan-based coating film, *Nanomaterials* 10 (7) (2020) 1365, <https://doi.org/10.3390/nano10071365>.
- [18] B. Yu, K.M. Leung, Q. Guo, W.M. Lau, J. Yang, Synthesis of Ag–TiO₂ composite nano thin film for antimicrobial application, *Nanotechnology* 22 (11) (2011), 115603, <https://doi.org/10.1088/0957-4484/22/11/115603>.
- [19] X. Zhang, G. Xiao, Y. Wang, Y. Zhao, H. Su, T. Tan, Preparation of chitosan-TiO₂ composite film with efficient antimicrobial activities under visible light for food packaging applications, *Carbohydr. Polym.* 169 (2017) 101–107, <https://doi.org/10.1016/j.carbpol.2017.03.073>.
- [20] A. Ashfaq, N. Khurshed, S. Fatima, Z. Anjum, K. Younis, Application of nanotechnology in food packaging: pros and Cons, *Journal of Agriculture and Food Research* 7 (2022), 100270, <https://doi.org/10.1016/j.jafr.2022.100270>.
- [21] N. Bumbudsanpharoke, S. Ko, Nano-food packaging: an overview of market, migration research, and safety regulations: an overview of nano-food packaging, *J. Food Sci.* 80 (5) (2015) R910–R923, <https://doi.org/10.1111/1750-3841.12861>.
- [22] D. Lin, Y. Yang, J. Wang, W. Yan, Z. Wu, H. Chen, Q. Zhang, D. Wu, W. Qin, Z. Tu, Preparation and characterization of TiO₂-Ag loaded fish gelatin-chitosan antibacterial composite film for food packaging, *Int. J. Biol. Macromol.* 154 (2020) 123–133, <https://doi.org/10.1016/j.ijbiomac.2020.03.070>.
- [23] S. Natarajan, M. Bhuvaneshwari, D.S. Lakshmi, P. Mrudula, N. Chandrasekaran, A. Mukherjee, Antibacterial and antifouling activities of chitosan/TiO₂/Ag NPs nanocomposite films against packaged drinking water bacterial isolates, *Environ. Sci. Pollut. Control Ser.* 23 (19) (2016) 19529–19540, <https://doi.org/10.1007/s11356-016-7102-6>.
- [24] R. Apjok, A. Mihaly Cozmuta, A. Peter, L. Mihaly Cozmuta, C. Nicula, M. Baia, A. Vulpoi, Active packaging based on cellulose-chitosan-Ag/TiO₂ nanocomposite for storage of clarified butter, *Cellulose* 26 (3) (2019) 1923–1946, <https://doi.org/10.1007/s10570-018-02226-7>.
- [25] A. Mihaly Cozmuta, R. Apjok, A. Peter, L. Mihaly Cozmuta, C. Nicula, M. Baia, A. Vulpoi, Active papers coated with chitosan and containing TiO₂ and Ag/TiO₂ nanoparticles for increasing the shelf-life of walnut kernels, *Cellulose* 25 (9) (2018) 5205–5225, <https://doi.org/10.1007/s10570-018-1925-x>.
- [26] K. He, N. Chen, C. Wang, L. Wei, J. Chen, Method for determining crystal grain size by X-ray diffraction, *Cryst. Res. Technol.* 53 (2) (2018), 1700157, <https://doi.org/10.1002/crat.201700157>.
- [27] E. Divsalar, H. Tajik, M. Moradi, M. Forough, M. Lotfi, B. Kuswandi, Characterization of cellulosic paper coated with chitosan-zinc oxide nanocomposite containing nisin and its application in packaging of UF cheese, *Int. J. Biol. Macromol.* 109 (2018) 1311–1318, <https://doi.org/10.1016/j.ijbiomac.2017.11.145>.
- [28] K.A.M. Amin, M.I.H. Panhuis, Reinforced materials based on chitosan, TiO₂ and Ag composites, *Polymers* 4 (1) (2012) 590–599, <https://doi.org/10.3390/polym4010590>.
- [29] Z. Deng, J. Jung, Y. Zhao, Development, characterization, and validation of chitosan adsorbed cellulose nanofiber (CNF) films as water resistant and antibacterial food contact packaging, *LWT - Food Sci. Technol. (Lebensmittel-Wissenschaft -Technol.)* 83 (2017) 132–140, <https://doi.org/10.1016/j.lwt.2017.05.013>.
- [30] J.J. Biemer, *Antimicrobial susceptibility testing by the Kirby-Bauer disc diffusion method*, *Ann. Clin. Lab. Sci.* 3 (2) (1973) 135–140.
- [31] J. Panigrahi, B. Gheewala, M. Patel, N. Patel, S. Gantait, Gibberellic acid coating: a novel approach to expand the shelf-life in green chilli (*Capsicum annum* L.), *Sci. Hortic.* 225 (2017) 581–588, <https://doi.org/10.1016/j.scienta.2017.07.059>.
- [32] B.S. Sooch, M.K. Mann, Nanoreinforced biodegradable gelatin based active food packaging film for the enhancement of shelf life of tomatoes (*Solanum lycopersicum* L.), *Food Control* 130 (2021), 108322, <https://doi.org/10.1016/j.foodcont.2021.108322>.
- [33] S. Pu, Y. Hou, H. Chen, D. Deng, Z. Yang, S. Xue, R. Zhu, Z. Diao, W. Chu, An efficient photocatalyst for fast reduction of Cr(VI) by ultra-trace silver enhanced titania in aqueous solution, *Catalysts* 8 (6) (2018) 251, <https://doi.org/10.3390/catal8060251>.
- [34] M. Hussain, S. Tariq, M. Ahmad, H. Sun, K. Maaz, G. Ali, S.Z. Hussain, M. Iqbal, S. Karim, A. Nisar, Ag TiO₂ nanocomposite for environmental and sensing applications, *Mater. Chem. Phys.* 181 (2016) 194–203, <https://doi.org/10.1016/j.matchemphys.2016.06.049>.
- [35] A. Yu Vakhrušev, T.B. Boitsova, TiO₂ and TiO₂/Ag nanofibers: template synthesis, structure, and photocatalytic properties, *J. Porous Mater.* 28 (4) (2021) 1023–1030, <https://doi.org/10.1007/s10934-021-01061-9>.
- [36] N. Rostami, M.G. Dekamin, E. Valiey, H. Fanimoghadam, Chitosan-EDTA-Cellulose network as a green, recyclable and multifunctional biopolymeric organocatalyst for the one-pot synthesis of 2-amino-4H-pyran derivatives, *Sci. Rep.* 12 (1) (2022) 8642, <https://doi.org/10.1038/s41598-022-10774-z>.
- [37] L. Calucci, C. Forte, Influence of process parameters on the hydrothermal carbonization of olive tree trimmings: a 13C solid-state nmr study, *Appl. Sci.* 13 (3) (2023) 1515, <https://doi.org/10.3390/app13031515>.
- [38] S.N. Sadikin, J. Ridwan, M.I.A. Umar, A.A.M. Raub, J. Yunas, A.A. Hamzah, D. Dahlan, M.Y.A. Rahman, A.A. Umar, Photocatalytic activity and stability properties of porous TiO₂ film as photocatalyst for methylene blue and methylene orange degradation, *Int. J. Electrochem. Sci.* 18 (9) (2023), 100246, <https://doi.org/10.1016/j.ijeecs.2023.100246>.
- [39] M. Sboui, H. Lachheb, S. Bouattour, M. Gruttadauria, V. La Parola, L.F. Liotta, S. Boufi, TiO₂/Ag₂O immobilized on cellulose paper: a new floating system for enhanced photocatalytic and antibacterial activities, *Environ. Res.* 198 (2021), 111257, <https://doi.org/10.1016/j.envres.2021.111257>.
- [40] Y. Jiao, C. Wan, J. Li, Anatase TiO₂/cellulose hybrid paper: synthesis, characterizations, and photocatalytic activity for degradation of indigo carmine dye, *Functional Materials Letters* 10 (3) (2017), 1750018, <https://doi.org/10.1142/S1793604717500187>.
- [41] K. Gupta, R.P. Singh, A. Pandey, A. Pandey, Photocatalytic antibacterial performance of TiO₂ and Ag-doped TiO₂ against *S. aureus*, *P. aeruginosa* and *E. coli*, *Beilstein J. Nanotechnol.* 4 (2013) 345–351, <https://doi.org/10.3762/bjnano.4.40>.
- [42] A.L.T. Zheng, S. Sabidi, T. Ohno, T. Maeda, Y. Andou, Cu₂O/TiO₂ decorated on cellulose nanofiber/reduced graphene hydrogel for enhanced photocatalytic activity and its antibacterial applications, *Chemosphere* 286 (2022), 131731, <https://doi.org/10.1016/j.chemosphere.2021.131731>.
- [43] F. Ahmadi, Z. Oveisi, S.M. Samani, Z. Amoozgar, Chitosan based hydrogels: characteristics and pharmaceutical applications, *Research in Pharmaceutical Sciences* 10 (1) (2015) 1–16.
- [44] S.J. Peighambari, S.H. Peighambari, N. Pournasir, P. Mohammadzadeh Pakdel, Properties of active starch-based films incorporating a combination of Ag, ZnO and CuO nanoparticles for potential use in food packaging applications, *Food Packag. Shelf Life* 22 (2019), 100420, <https://doi.org/10.1016/j.fpsl.2019.100420>.
- [45] H. Hajizadeh, S.J. Peighambari, S.H. Peighambari, D. Peressini, Physical, mechanical, and antibacterial characteristics of bio-nanocomposite films loaded with Ag-modified SiO₂ and TiO₂ nanoparticles, *J. Food Sci.* 85 (4) (2020) 1193–1202, <https://doi.org/10.1111/1750-3841.15079>.
- [46] S. Sänglerlaub, M. Schmid, K. Müller, Comparison of water vapour transmission rates of monolayer films determined by water vapour sorption and permeation experiments, *Food Packag. Shelf Life* 17 (2018) 80–84, <https://doi.org/10.1016/j.fpsl.2018.06.004>.
- [47] M. Yamaguchi, H. Abe, T. Ma, D. Tadaki, A. Hirano-Iwata, H. Kanetaka, Y. Watanabe, M. Niwano, Bactericidal activity of TiO₂ nanotube thin films on Si by photocatalytic generation of active oxygen species, *Langmuir* 36 (42) (2020) 12668–12677, <https://doi.org/10.1021/acs.langmuir.0c02225>.

- [48] Y. Xing, H. Yang, X. Guo, X. Bi, X. Liu, Q. Xu, Q. Wang, W. Li, X. Li, Y. Shui, C. Chen, Y. Zheng, Effect of chitosan/Nano-TiO₂ composite coatings on the postharvest quality and physicochemical characteristics of mango fruits, *Sci. Hortic.* 263 (2020), 109135, <https://doi.org/10.1016/j.scienta.2019.109135>.
- [49] Y. Xing, S. Yang, Q. Xu, L. Xu, D. Zhu, X. Li, Y. Shui, X. Liu, X. Bi, Effect of chitosan/nano-TiO₂ composite coating on the postharvest quality of blueberry fruit, *Coatings* 11 (5) (2021) 512, <https://doi.org/10.3390/coatings11050512>.
- [50] C. López De Dicastillo, M. Guerrero Correa, F. B. Martínez, C. Streitt, M. José Galotto, Antimicrobial effect of titanium dioxide nanoparticles, in: M. Mareş, S. Hua Erin Lim, K.-S. Lai, R.-T. Cristina (Eds.), *Antimicrobial Resistance—A One Health Perspective*, IntechOpen, 2021, <https://doi.org/10.5772/intechopen.90891>.